PASJ: Publ. Astron. Soc. Japan **53**, 517–533, 2001 June 25

Kashima 34-m Water Maser Survey of Late-Type Stars

Hiroshi TAKABA,[1,2] Takahiro IWATA,[1,3] Takeshi MIYAJI,[4,5] and Shuji DEGUCHI[4]
[1]*Kashima Space Research Center, Communications Research Laboratory, Kashima, Ibaraki, 314-0012*
[2]*Department of Civil Engineering, Faculty of Engineering, Gifu University, Yanagito 1-1, Gifu-city, Gifu 501-1193*
takaba@cc.gifu-u.ac.jp
[3]*Office of Research & Development, National Space Development Agency of Japan, Tsukuba, Ibaraki 305-8505*
[4]*Nobeyama Radio Observatory, National Astronomical Observatory, Minamimaki, Minamisaku, Nagano 384-1305*
[5]*VERA Project Office, National Astronomical Observatory, Mitaka, Tokyo 181-8588*

(Received 2000 December 20; accepted 2001 March 19)

Abstract

This paper presents new results of a water maser survey of late-type stellar objects at 22.235 GHz with the Kashima 34-m radio telescope. We have detected 179 out of 643 observed sources, including 32 new detections. The sources were selected in terms of the IRAS flux density and colors of late-type stars, involving optically observable Mira/semiregular variables, IRC objects, OH/IR sources and protoplanetary nebulae. We found the highest H_2O detection rate for the type of stars with a thin dust envelope (Mira/semiregular variables) among other types of sources. This is attributed to the smaller distances to such stars in the sample. The velocity spread of the H_2O maser profile has an increasing tendency with the IRAS color, though it becomes more difficult to access this color dependence beyond an edge of the transition of the (oxygen-rich) Asymptotic Giant Branch stars to protoplanetary nebulae in the two-color diagram.

Key words: masers — radio lines: stars — stars: circumstellar shells — stars: late-type — stars: mass-loss

1. Introduction

Water masers as well as OH and SiO masers have been used as a probe of circumstellar envelopes of late-type stars (Reid, Moran 1981). The H_2O maser is emitted in the envelope at a radius of $\sim 10^{14}$–10^{15} cm, slightly outside of the SiO maser emitting region, but considerably inside of the OH 1612 MHz maser emitting region (Deguchi 1977). Large surveys of late-type steller objects in the 22 GHz H_2O line have been made (e.g., Takaba et al. 1994) and stellar maser sources have been cataloged extensively (Benson et al. 1990; Brand et al. 1994). The catalogs involve a variety of objects from optically observable Mira and semiregular variables, optically unseen IRC objects, OH/IR objects and protoplanetary nebulae. These are all Asymptotic Giant Branch stars (AGB) and post-AGB objects. It is known that the H_2O maser intensity in these objects is time-variable. Therefore, even though plenty of H_2O maser searches have already been performed, a number of new detections can be expected by repeating observations. For surveying H_2O masers, we made an automated H_2O maser survey system in the Kashima 34-m antenna in 1991. The survey was made several times first in 1991 spring (Takaba et al. 1994) and later during the season from 1991 autumn to early 1992. In the 1991–1992 survey, the observations were repeated at least twice with a time interval of one month for most of the sources. This survey resulted in a number of new detections in H_2O masers for the color-selected IRAS objects. Time has passed since this survey observation was completed; some of new detections originally involved in this survey have been reported by others (e.g., Lewis 1997a). However, this survey still includes many first detections of H_2O masers in late-type stars. Therefore, we decided to publish the results in this paper.

2. Observations

The observations in the H_2O 6_{16}–5_{23} transition at 22.235 GHz were made between 1991 October and 1992 January with the 34-m radio telescope at Kashima Space Research Center, Communications Research Laboratory. The receiver was a HEMT amplifier working at 22 GHz with T_{sys} = 140–180 K. The aperture efficiency of the telescope was about 0.57. A portable acousto-optical spectrometer with 2048 channels with a bandwidth of 40 MHz was equipped. The velocity resolution and coverage were 0.52 and 540 km s^{-1}, respectively. The observations were made by position switching with the off-positions at 10′ away from the source position. The integration time was typically 10 min for each source and the RMS noise level was about 0.2 Jy per channel. The integration was repeated when a weak signal was detected. The telescope half-power beam width (HPBW) was 1′.6. Because the details of the system are described in Takaba (1991) and Takaba et al. (1994), they are not repeated here.

The sources were chosen from the IRAS Point Source Catalog. The selections were made by IRAS colors of late-type stars in terms of $\log(F_{25}/F_{12}) \equiv C_{12}$, and $\log(F_{60}/F_{25}) \equiv C_{23}$ (cf. van der Veen, Habing 1988) and F_{12}, where F_{12}, F_{25}, and F_{60} are the IRAS flux densities at 12, 25, and 60 μm, respectively. We have chosen the sources in the three areas in the two-color diagram in figure 1: the rectangular region ($-0.48 < C_{12} < -0.2$ and $-1 < C_{23} < -0.6$; Type 1) is the class of optically observable Mira and semi-regular variables (corresponding region VII in van der Veen, Habing 1988); the square region ($-0.2 < C_{12} < 0.2$ and $-1 < C_{23} < -0.6$; Type 2) is the class of optically unseen IRC objects (corresponding region IIIa in van der Veen, Habing 1988); and the polygo-

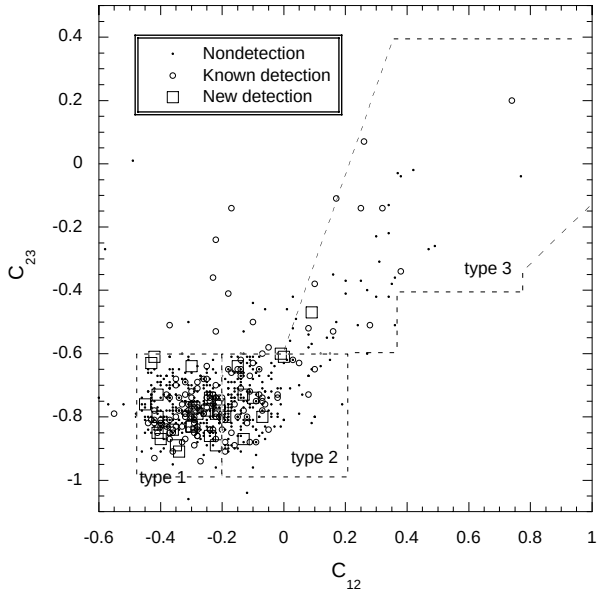

Fig. 1. Two-color diagram of the observed sources. The squares, circles, and dots indicate the new detections, the previously known detections, and non-detections in H_2O. The sources are divided into three types according to their IRAS color. There are 6 detected sources out of this figure.

nal region ($0 < C_{12} < 1$; see figure 1, Type 3) is the area of the OH/IR sources and proto-planetary nebulae (corresponding parts of regions IIIb, IV, V, VIb, IV, and VIII in van der Veen, Habing 1988). In total, about 8700 sources were chosen. We have also selected several interesting sources (known H_2O detections) out of this area. The observations were automated and programed to observe sources according to the priorities depending on the weather. In total, 500 hours were spent for qualified observations at 22 GHz. The observed positions were the IRAS PSC positions for all of the sources. We show the positions of the observed sources in the two-color diagram in figure 1.

In total, 643 sources were observed in H_2O and 179 were detected, including 32 new detections. The parameters of the detected lines are summarized in table 1 for new detections, and in table 2 for previously known detections. Table 3 gives the upper limit of the flux density for non-detections. The 4th column in tables 1 and 2 specifies the type of spectrum (sp), i.e., the single (S), double (D) and multiple (M) peaks of the H_2O profile. For the single-peak sources, the line was fitted by a Gaussian function; the resulting peak flux density, the peak radial velocity, and the e^{-1} width are listed in tables. For double-peak sources, each peak was fitted by a Gaussian function; the peak flux density of the stronger peak and the middle velocity of the two peaks, as well as the separation in velocity of the two peaks are given in tables 1 and 2. For multiple-peak sources, the strongest peak intensity, the average velocity of several peaks, and the largest separation in velocity between the peaks are listed. The detections were first judged by eye and then selected by a criterion of the signal-to-noise ratio being above 5. The previous detections were checked in Benson et al. (1990), the Arcetri H_2O maser catalog (Brand et al. 1994), and the SIMBAD database. The numbers of Type-1, -2, and -3 sources are 362, 232, and 48, respectively, and the numbers of detections are 111, 52, 15, respectively (we excluded one source, NML Cyg, from the statistics, which is not in the IRAS PSC catalog). The spectra of 32 new H_2O detections are shown in figure 2. We also checked table 1 (the target list of OH main line search) of Lewis et al. (1995), and found that several sources were assigned as D (detection of H_2O), but no literature was given; these are 03318−1619, 06193−0349, 17048−1601, 17139+0446, 20038−2722, and 21439−0226. These are probably the sources observed at Haystack as cited as "Lewis, B. 1995 (Haystack observatory)" in Lewis et al. (1995) without any further information. We included these sources into new detections.

2.1. *Individual Sources*

Here, individually interesting sources are discussed. The observed radial velocities of H_2O masers were compared with the radial velocities of SiO/OH masers; it was confirmed that they coincide well within a few $\mathrm{km\,s^{-1}}$ accuracy, except for one source, 21439−0226, as discussed below.

07051+6601: The SIMBAD database assigned this sources as HD 53469 with *B* magnitude 9.9, a variable star with spectral type K0. However, the position of this star is $1'50''$ north of the IRAS PSC position. Therefore, HD 53469 is probably not the IRAS counterpart. The IRAS LRS class of this star is 29, indicating strong silicate emission. Table 1 of Lewis et al. (1995) gives "D" (detection of H_2O) for this source, but we could not find any literature for it. The OH main-line and CO searches were negative (Lewis et al. 1995; Nyman et al. 1992).

18056−1954: This source (OH 10.4+0.0) exhibits a slightly odd IRAS color $(C_{12}, C_{23}) = (0.82, 2.26)$. The OH 1612 MHz double peaks were detected by Baud et al. (1979). The Arcetri H_2O maser catalog (Cesaroni et al. 1988) gave two H_2O sources nearby ($3'$ separation): one is assigned as "Star", and the other "Star Forming Region" (W 31; Genzel, Downes 1977) and the radial velocities of the H_2O line are almost the same ($V_{\mathrm{lsr}} \simeq 64\,\mathrm{km\,s^{-1}}$). The IRAS position observed is near the middle of these two sources, suggesting that the detection of H_2O might be a contamination by the above two sources; the broad feature of the H_2O spectrum in figure 2 also indicates that the H_2O emission from the W 33 star forming region was detected from the lobe of the telescope beam. However, a medium bright star with a color of late-type stars can be found at the IRAS position (within a few arcsec) in the 2MASS archive *JHK* images (Skrutskie et al. 2000). It is thus possible that the star position in the Arcetri H_2O maser catalog is somewhat inaccurate. More precise observations are necessary for this source.

18076−1034: NSV 10306 (= IRC−10401). Stephenson (1990) classified this star as M7S-type. IRAS LRS class is 28, indicating a strong silicate emission. Hall et al. (1990b) detected the SiO $J = 1$–0 $v = 1$ line, and Groenewegen, de Jong (1998) detected CO $J = 1$–0 and 2–1 lines from this star at $V_{\mathrm{lsr}} \simeq 20\,\mathrm{km\,s^{-1}}$. They are consistent with the H_2O detection at $V_{\mathrm{lsr}} \simeq 19.7\,\mathrm{km\,s^{-1}}$.

19075+0921: This source has the IRAS color $(C_{12}, C_{23}) = (0.08, -0.47)$, a typical color of late-type steller objects. Meixner et al. (1999) included this source in their

Table 1. List of new detections.

IRAS name	Star name	Type	Peak	S	V_{lsr}	ΔV	Obsd1	Obsd2	SiO	OH	Reference
				(Jy)	(km s^{-1})	(km s^{-1})	(yymmdd)	(yymmdd)			
03287−1535	ET Eri	2	S	10.0	−5.6	2.3	911115	911220		Y	L92
03318−1619	RT Eri	1	S	1.3	24.1	3.0	911112	···		Y	L95(D)
03599+1632	TZ Tau	1	S	4.2	8.2	3.0	911023	911030			T94
05404−2343	RT Lep	1	S	14.2	66.0	4.2	920119	···	Y	N	H94,T91
05450−3142	S Col	1	S	6.5	62.4	2.6	911106	911109	Y	Y	S89
06193−0349	IRC+00102	2	S	1.6	−16.0	1.7	911115	911220		Y	L95(D)
06423+0905	FX Mon	1	S	1.5	33.4	2.2	911029	911123		Y	S89
07051+6601	IRC+70074	1	M	1.7	7.1	6.6	920112	920119		N	N92,L95
10189−3432	V Ant	1	S	20.7	−18.6	1.8	911106	911123	N	Y	H90a,S89
14020−3515	AQ Cen	1	S	1.3	2.4	1.8	911112	911113	Y	Y	H90a,L95
16574−1032	IRC−10355	1	M	1.2	−48.9	4.3	920113	···		N	T91,L97a
17043−3145	TU Sco	1	S	2.7	−14.0	1.2	911111	···		Y	S89,B90
17048−1601	R Oph	1	S	2.1	−37.3	1.1	911106	···	Y		B85, L95(D), L97a(D)
17139+0446	UY Oph	1	S	1.5	−68.9	2.8	920112	···		N	L94,L95(D)
17436−1545	17436−1545	2	D	2.3	13.6	23.4	911115	···	Y	Y	I95,T91
18056−1954	OH10.4+0.04	3	M	2.2	64.4	9.8	911111	···		Y	T89
18076−1034	IRC−10401	1	S	2.2	19.7	1.6	911112	911114	Y	N	H90b,T91
18125+3010	IRC+30330	1	D	1.0	−10.4	7.4	920111	920119		N	L94
18139−1811	18139−1811	2	S	4.6	29.3	1.7	911118	···		Y	T91,L92
18141+0340	RY Oph	1	S	1.9	−55.7	0.5	911030	911107	Y		J91
18248−1229	UY Sct	2	M	10.5	26.6	4.5	911114	···		N	T91
18429−1721	18429−1721	1	D	10.7	−3.9	7.8	920114	···		Y	T91,L95
19075+0921	19075+0921	3	M	1.5	7.6	8.5	911116	920119	N	Y	N98, L92
19247−1722	IRC−20563	1	D	19.2	−33.4	7.5	920119	···	N	N	H94,T91
19354+5005	R Cyg	1	S	1.0	64.3	2.9	911112	911113	Y		B96
19374+0550	19374+0550	2	S	4.9	−27.2	1.9	911114	911124		Y	L90,L95(D)
20038−2722	V 1943 Sgr	1	S	1.9	−17.4	2.5	911112	911124	Y		H94,L95(D)
20094−1121	IRC−10530	1	S	3.6	−21.9	1.2	920112	···		N	T91
20296−2151	RU Cap	2	S	3.2	7.2	1.7	911116	···	Y	Y	T91,D01,L95(D)
21100−1435	21100−1435	1	S	14.2	−54.0	2.3	920112	···	N		H94
21439−0226	EP Aqr	1	S	1.7	−70.8	1.1	911113	···	Y	N	H94, L95(D), L97a(D)
22048+5914	NSV 25835	2	S	1.2	−61.2	2.7	911114	···			

References; B79–Baud et al. (1979), B90–Benson et al. (1990), B96–Bujarrabal et al. (1996), D01–Deguchi et al. (2001), H90a–Hall et al. (1990a), H90b–Hall et al. (1990b), H90c–Haikala (1990), H94–Haikala et al. (1994), I95–Izumiura et al. (1995), J91–Jewell et al. (1991), L92–Le Squeren et al. (1992), L95–Lewis et al. (1995), L97a–Lewis (1997a), L97b–Lewis (1997b), N92–Nyman et al. (1992), N98–Nyman et al. (1998), T89–te Lintel-Heckert et al. (1989), T91–te Lintel Hekkert et al. (1991), T94–Takaba et al. (1994), S89–Sivagnanam et al. (1989), The "D" sign in the parentheses indicates the H_2O detection noted in the cited paper, but no data available.

protoplanetary-candidate list and assigned it as C-rich. The IRAS LRS class is 12, indicating a flat spectrum. OH masers have been detected at velocity V_{lsr} = 12.3 km s^{-1} (Le Squeren et al. 1992), which is consistent with the H_2O V_{lsr} = 7.6 km s^{-1}. The SiO J = 1–0 v = 2 search was negative (Nyman et al. 1998).

19354+5005: The SIMBAD database assigned this source as HD 185456 (R Cyg), a star with spectral type S2.5–S9. Previous searches for the H_2O maser of this star were negative (Benson, Little-Marenin 1996). Though the SiO maser of the J = 2–1, v = 1 transition has been detected, the SiO J = 2–1, v =2 transition was not (Bujarrabal et al. 1996). The detection of the H_2O maser and the non-detection of the SiO J = 2–1 and v = 2 transition in this star is consistent with the suppression mechanism of the SiO J = 2–1 and v = 2 masers by the line overlap of H_2O and SiO vibration–rotation transitions. (Bujarrabal et al. 1996).

21439−0226: This is EP Aqr (= HD 207076), a M8 III star. Strong CO_2 emission has been detected with the ISO Short Wavelength Spectrometer (Cami et al. 2000), and CN and NH bands have been observed from the ground (Aoki, Tsuji 1997). Table 2 (H_2O negative result) of Lewis (1997a) gave the "D" sign (H_2O detection) for this source, but we do not find any report of H_2O detection for it. The search for OH 1612 MHz and main lines was negative (Lewis et al. 1995). The J = 2–1 v = 1 SiO maser was detected at V_{lsr} = −35 km s^{-1} (Haikala et al. 1994). The CO J = 1–0 emission has been detected at V_{lsr} = −35 km s^{-1} with the expansion velocity of 11 km s^{-1} (Nyman et al. 1992). The H_2O radial velocity of V_{lsr} = −70 km s^{-1} observed in the present paper seems to be considerably lower than the SiO and CO radial velocities. Further observations are necessary for this source.

Table 2. List of known detections.

IRAS name	Star name	Type	Peak	S	V_{lsr}	ΔV	Obsd1	Obsd2	H_2O Reference
				(Jy)	(km s^{-1})	(km s^{-1})	(yymmdd)	(yymmdd)	
00007+5524	Y Cas	1	S	2.8	−17.8	2.7	911023	920111	B94
00050−2546	SY Scl	1	S	0.8	21.7	4.0	911029	911105	B94
00340+6251	TY Cas	1	S	1.7	−58.9	1.8	911023	911123	B94
00428+6854	V 524 Cas	2	M	1.3	−25.9	22.0	911023	911220	B94
01037+1219	WX Psc	2	S	0.8	−2.2	3.6	911023	911220	E96
01556+4511	IRC+50049	1	D	2.0	−4.7	8.7	911022	911111	B94
02168−0312	o Cet	1	S	1.2	46.4	2.2	911029	911111	B94
02192+5821	S Per	2	D	17.4	−39.4	12.4	911113	911123	B94
02351−2711	IRC−30023	1	M	2.0	−5.4	3.7	911029	911111	D89
02404+2150	02404+2150	1	M	3.5	−45.5	7.4	911106	911110	E96
02420+1206	RU Ari	1	S	7.7	19.4	1.9	911029	911105	E96
02587+2136	UZ Ari	1	S	2.5	−38.2	2.4	911106	911109	B94
03507+1115	IK Tau	1	D	20.2	37.1	14.4	911030	911112	B94
03598−1353	WZ Eri	1	M	2.5	5.0	8.5	911029	···	B96
04094−2515	W Eri	1	S	6.5	−0.4	1.5	911105	920119	B94
04166+4056	IR Per	1	S	1.2	−29.6	1.8	911111	911114	S95
04255+1003	R Tau	1	S	1.7	13.8	2.8	911022	920113	B94
04280+2722	V 729 Tau	1	S	1.6	−6.5	1.2	911106	911110	B94
04311−0004	BD Eri	1	S	2.0	−12.0	1.6	911029	911105	B96
04382−1417	BX Eri	1	S	7.7	−3.9	1.5	911111	911115	S97
04387−3819	R Cae	1	S	1.3	0.2	1.8	911106	911112	B84
05027−2158	T Lep	1	D	21.0	−28.2	4.6	911105	911111	B94
05151+6312	IRC+60154	1	D	3.8	51.6	15.3	911023	911111	B94
05365−1404	RW Lep	1	S	3.3	−58.0	2.3	911105	920113	B94
05388+3200	U Aur	1	S	8.6	5.2	2.4	911111	911123	B94
05411+6957	IRC+70066	1	D	2.7	67.9	20.5	911023	911029	B94
05443+2707	AW Tau	1	S	4.1	−12.3	1.2	911023	911123	B94
05528+2010	U Ori	1	S	2.9	−38.1	2.1	911111	911123	B94
05535+4822	LO Aur	2	D	11.5	−2.0	5.4	911106	911115	B96
06300+6058	IRC+60169	2	D	16.3	−27.5	13.8	911030	911113	B94
06319−0501	AFGL 5201	3	S	7.2	−61.6	1.1	911106	911109	B94
06363+5954	U Lyn	1	D	14.3	−14.5	8.0	911112	911123	B94
06500+0829	GX Mon	1	S	2.4	−1.2	1.8	911029	911123	B94
07054−1039	IRC−10151	2	D	2.4	50.5	9.0	911105	911220	B94
07209−2540	VY CMa	2	M	1238.0	16.9	3.4	911029	911220	B94
07304−2032	Z Pup	1	S	1.7	−3.9	1.9	911105	911111	B94
07308+3037	IRC+30187	1	D	31.4	3.9	20.9	911024	911123	B94
07399−1435	QX Pup	3	S	4.2	22.1	4.1	911029	···	B94
07445−2613	SS Pup	1	S	10.6	82.0	2.6	920119	···	H98
07446−3210	07446−3210	2	M	25.2	25.1	11.2	911106	911113	D89
07536−2830	HU Pup	2	S	13.7	43.0	6.2	911106	911220	S95
08357−1013	OH235.3+18.1	2	S	1.5	66.6	6.0	911029	911220	B94
08534−1901	IRC−20176	1	S	3.9	5.1	3.4	911029	911105	B94
09069+2527	W Cnc	1	S	2.6	35.6	1.2	911123	920111	B94
09235−2347	IRC−20188	2	D	5.4	6.1	16.0	911029	911220	B94
09331−1428	X Hya	1	S	1.6	26.2	3.3	911105	920112	B94
09425+3444	R LMi	1	S	7.4	−0.6	3.6	911024	911112	B94
10521+7208	VX UMa	1	S	2.5	−50.5	2.8	911107	911124	B94
10580−1803	R Crt	1	M	134.9	8.7	7.3	911022	911105	B94
11501−0719	S Crt	1	D	102.5	40.1	2.0	911105	920113	B94
12120−0545	T Vir	1	S	3.2	6.7	2.1	911022	911024	B94
12562+2324	T Com	1	S	2.1	25.7	1.7	911022	911105	B94
13001+0527	RT Vir	1	D	94.3	17.3	11.5	911022	911112	B94
13269−2301	R Hya	1	S	2.6	−10.9	2.9	911105	911111	B94

Table 2. (Continued)

IRAS name	Star name	Type	Peak	S	V_{lsr}	ΔV	Obsd1	Obsd2	H_2O Reference
13462−2807	W Hya	1	D	47.5	39.7	3.4	911023	911123	B94
13492−0325	AY Vir	1	S	5.9	−42.4	2.2	911022	911105	B94
14086−0730	OH334.8+50.1	2	D	1.9	-26.0	16.7	911115	911220	B96
14086−2839	RU Hya	1	S	5.9	−3.7	3.7	911123	920112	B94
14219+2555	RX Boo	1	S	5.3	0.9	2.5	911105	911112	B94
14247+0454	RS Vir	1	S	10.5	−14.6	1.7	911105	911112	B94
15060+0947	15060+0947	2	S	11.7	−14.4	2.6	911114	911124	B94
15090−0549	Y Lib	1	S	6.0	13.2	3.6	911023	911106	B94
15193+1429	S Ser	1	D	1.5	20.3	6.6	911023	911124	B94
15193+3132	S Crb	1	S	16.1	0.8	1.9	911112	911123	B94
15194−1829	IRC−20285	1	S	3.4	−7.4	1.8	911109	···	B94
15255+1944	WX Ser	2	D	22.6	3.3	9.0	911029	911220	B94
15298+0348	WW Ser	1	S	6.0	20.1	3.3	911106	911124	B94
15410−0133	BG Ser	1	S	1.5	−2.3	6.2	911112	911115	L97
15528−1242	SW Lib	1	S	2.7	−20.1	1.4	911109	911123	B94
15576−1212	FS Lib	1	S	8.0	−4.5	2.7	911106	911123	B94
16011+4722	X Her	1	D	1.8	−76.1	7.0	911112	911116	B94
16029−3041	OH345.0+15.7	3	S	2.1	7.5	1.3	911109	920113	B94
16235+1900	U Her	1	S	71.3	−19.4	2.6	911029	911123	B94
16306+7223	R UMi	1	S	5.4	−8.9	1.5	911022	911123	B94
16503+0529	RX Oph	1	S	14.2	−48.0	1.3	911030	911123	B94
17034−1024	V 850 Oph	1	S	3.3	1.8	1.8	911106	911123	T94
17080−3215	AH Sco	1	M	49.1	−4.1	9.5	911111	911112	B89
17115−3322	RW Sco	1	S	8.5	−72.4	4.9	911111	911112	B90
17119+0859	IRC+10322	2	M	27.3	13.0	12.1	911116	911123	B94
17162−1934	V 1848 Oph	1	M	1.3	−21.9	16.2	920113	···	B96
17229−0301	AH Oph	1	S	35.3	51.0	1.1	911109	911123	B94
17230+0113	17230+0113	2	S	3.5	−31.4	1.7	911106	911123	B94
17354−3155	IRC−30308	2	M	12.9	2.6	2.4	911106	911124	T94
17376−3021	OH358.23+0.11	2	M	41.6	−6.4	7.1	911105	···	T94
17393−3004	OH358.67−0.04	2	M	25.4	−16.9	12.7	911105	···	T94
17484−0800	V 2211 Oph	2	S	25.5	−21.2	1.8	911030	911118	B94
17501−2656	OH2.58−0.43	2	D	18.9	−3.9	29.4	911105	911124	B94
17579+2335	WY Her	1	S	3.2	2.5	1.9	911106	920119	B94
18009−2019	IRC−20424	2	D	2.8	11.9	12.0	911030	···	B94
18018−2802	V 1804 Sgr	1	S	30.2	19.3	2.2	911105	911112	T94
18025−2113	IRC−20427	2	D	3.8	5.5	17.4	911030	···	B94
18039−0813	IRC−10395	1	S	5.0	20.1	1.5	911109	920113	B94
18050−2213	VX Sgr	1	M	103.7	−3.0	6.5	911105	911113	B94
18135−1641	IRC−20454	2	M	29.4	39.5	25.2	911105	911124	B94
18176−1848	OH12.8−1.9	3	D	19.9	9.8	19.5	911022	920119	B94
18186+3143	TU Lyr	1	S	2.7	9.0	1.9	920111	920119	S97
18204−1344	IRC−10414	2	D	33.0	39.0	14.8	911114	920119	B94
18213+0335	V 2090 Oph	1	D	1.8	−28.6	9.1	920119	···	L97,S97
18252−1305	18252−1305	1	M	17.8	37.8	1.2	920113	···	H98
18327−0715	OH24.7+0.2	3	D	8.3	43.1	31.7	911105	911127	B90
18340−0720	OH24.7−0.1	0	S	2.2	73.1	3.5	911109	911124	B90
18348−0526	V 437 Sct	3	D	1.3	39.8	9.9	911022	911030	B94
18349+1023	V 1111 Oph	1	S	7.3	−44.8	2.1	911029	911112	B94
18385−0617	V 438 Sct	3	S	5.9	55.0	2.4	911105	···	B94
18387−0423	IRC+00363	2	M	36.0	46.7	13.0	911109	···	B94
18395−0248	IRC+00364	2	M	10.4	56.3	14.2	911109	911124	B94
18413+1354	IRC+10374	2	M	4.0	−13.8	14.5	911022	911116	B94
18436+4334	RW Lyr	2	D	48.5	−25.3	8.2	911124	920111	B94
18560+0638	V 1366 Aql	3	S	1.7	17.2	1.2	911123	920119	B94

Table 2. (Continued)

IRAS name	Star name	Type	Peak	S	V_{lsr}	ΔV	Obsd1	Obsd2	H_2O Reference
18596+0315	OH37.1−0.8	3	S	2.6	65.6	5.0	911109	911124	E96
19039+0809	R Aql	1	S	26.6	46.9	2.8	911022	911123	B94
19061+1041	19061+1041	2	S	3.0	22.3	2.2	911106	911111	B94
19069+0916	19069+0916	3	D	4.9	−11.6	41.2	911106	911111	B94
19083+0851	19083+0851	2	D	5.5	32.9	51.2	911116	···	E96
19110+1045	OH45.07+0.13	3	M	21.5	63.6	2.4	911111	911123	B94
19229+1708	19229+1708	2	M	7.9	40.6	19.4	911116	911124	E96
19243+7135	YZ Dra	1	S	3.4	−36.6	0.8	911106	911123	B94
19296+4331	UV Cyg	1	D	2.9	18.2	13.0	911112	911113	S95
19356+1136	RT Aql	1	S	101.1	−30.7	1.7	911022	920112	B94
19361−1658	OH22.7−17.9	2	M	2.4	54.9	8.7	911109	911124	B96
19387+1527	19387+1527	2	S	2.4	52.6	6.0	911107	···	E96
19412+0337	IRC+00450	1	S	1.4	−36.7	1.3	911112	911114	E96
19422+3506	AFGL 2455	2	S	2.0	−57.3	1.3	911117	···	E96
19495+0835	19495+0835	2	D	2.8	45.9	7.4	911107	911116	B94
19536+3237	V 468 Cyg	1	S	1.7	−46.4	2.8	911106	911112	B94
19550−0201	RR Aql	1	S	174.7	26.9	2.5	911112	911124	B94
19566+3423	19566+3423	3	S	1.3	−39.0	2.1	920112	···	B94
20015+3019	20015+3019	2	D	21.6	18.4	3.4	911113	···	E96
20047+1248	SY Aql	1	S	10.8	−47.7	1.7	911124	920112	B94
20109+3205	V 557 Cyg	1	S	14.5	53.4	1.1	920112	···	B96
20125+0856	R Del	1	S	2.5	−31.9	1.5	911030	911124	B96
20241+3811	KY Cyg	2	S	3.5	−12.5	1.8	911022	911113	B94
20363+3401	20363+3401	2	S	1.9	12.3	2.4	911107	911109	B94
20445+3955*	NML Cyg	0	D	35.6	−7.8	25.5	911022	911105	B94
20491+4236	OH83.42−0.89	2	S	3.1	−49.0	3.1	911106	911109	B94
20529+3013	UX Cyg	1	D	22.9	−3.9	4.4	911022	911030	B94
21086+5238	IRC+50362	1	S	0.9	−11.2	4.0	920113	···	L97
21426+1228	TU Peg	1	S	9.1	9.9	1.9	911022	920112	B96
22035+3506	SV Peg	1	D	4.3	7.5	9.2	911030	911112	S95
22512+6100	V 386 Cep	2	D	13.9	−52.9	6.9	911113	···	H98
22516+0838	IRC+10523	1	S	3.5	−3.9	1.3	911112	···	B94
22525+6033	MY Cep	2	D	3.8	−55.8	12.7	911030	911113	B94
22556+5833	V 627 Cas	2	M	7.1	−47.0	4.4	911113	911123	B94
23041+1016	R Peg	1	S	6.7	24.4	1.8	911105	911112	B94
23182+3920	RY And	1	S	1.2	0.0	3.2	911022	911030	B94
23416+6130	PZ Cas	2	D	4.6	−42.8	2.2	911022	920111	B94
23558+5106	R Cas	1	S	2.7	25.8	3.3	911022	911111	B94

* This source was not found in the IRAS Point Source Catalog so that we excluded this source from the statistical analysis in the present paper.
Reference; B84– Bowers and Hagen (1984), B89–Barvainis and Deguchi (1989), B90–Benson et al. (1990), B94–Brand et al. (1994), B96–Benson and Little-Marenin (1996), D89–Deguchi et al. (1989), E96–Engels and Lewis (1996), H98–Han et al. (1998), S95–Szymczak and Engels (1995), S97–Szymczak and Engels (1997), and T94–Takaba et al. (1994).

3. Discussion

Here we will discuss the IRAS properties, the H_2O detection rate, the velocity width, and the galactic distribution of the observed sources.

3.1. IRAS Properties of the Sample

We made histograms of the IRAS 12 μm flux density (top), and colors, C_{12} (middle) and C_{23} (bottom), for the detected and undetected sources in figure 3a. The detection rates are also shown as line graphs (the scale shown on the right vertical axis). The average detection rate was about 28%. The detection rate seems peaked at the range $C_{12} \sim -0.4$ to -0.2. Figure 3a shows no clear tendency in the detection rate, except for a small drop in the detection rate at $C_{23} \sim -0.7$ to -0.6. Because the number of sampled stars decreases at the right half of the horizontal axis, the statistics is somewhat uncertain there; the high peaks of the detection rate in the right half of the histograms are artifacts due to poor statistics. These panels rather seem to be characterized by a flat detection rate in F_{12}, C_{12} and C_{23}. Because the range of the IRAS color, C_{12}, spreads widely, the flux density, F_{12}, is not necessarily a good indicator of distance in this case.

It is expected that the detection rate is somewhat dependent on the types of sources. The average detection rates are 31, 22, and 31% for type-1, -2 and -3 sources, respectively. The low detection rate for type-2 sources is surprising, because this color range for the type-2 sources, $-0.2 < C_{12} < 0.2$, is a

Table 3. List of nondetections.

IRAS name	Star name	Type	$S \leq$	Obsd1	Obsd2
			(Jy)	(yymmdd)	(yymmdd)
00017+3949	SV And	1	0.7	911023	911105
00042+4248	KU And	2	0.5	911115	911220
00067+6340	V 641 Cas	1	0.5	920111	···
00127+5437	00127+5437	2	0.5	911114	···
00128−3219	S Scl	1	0.8	911109	911112
00170+6542	OH119.7+3.3	2	0.9	911106	911123
00205+5530	T Cas	1	0.9	911023	911111
00213+3817	R And	1	0.7	911105	911111
00245−0652	UY Cet	1	1.1	911112	···
00247+6922	00247+6922	1	0.9	911111	···
00479+4614	00479+4614	2	0.7	911115	···
00506+5224	00506+5224	2	0.4	911114	911115
01010+7434	01010+7434	1	0.4	920111	···
01085+3022	IRC+30021	2	0.4	911023	911220
01144+6658	01144+6658	3	0.4	911116	920111
01150+5732	01150+5732	1	0.4	920111	···
01159+7220	S Cas	1	0.9	911023	911111
01304+6211	OH127.8−0.0	3	0.4	911029	911116
01438+1850	SV Psc	1	0.7	920113	···
01597+5459	XX Per	1	0.5	920111	···
02143+4404	W And	1	0.8	911030	911111
02153+5711	BU Per	2	0.7	911113	···
02188+5652	RS Per	2	0.4	911113	911220
02234−0024	R Cet	2	0.8	911029	911105
02236+6027	IRC+60091	2	0.3	911113	911220
02251+5102	RR Per	1	0.5	911023	920112
02302+4525	UX And	1	0.9	911111	···
02313−1322	U Cet	1	0.7	911029	911105
02316+6455	IRC+60092	2	0.6	911023	911113
02339+3402	R Tri	1	1.4	911023	911030
02347+5649	YZ Per	2	0.8	911113	···
02361+8055	RR Cep	1	0.9	911023	911123
02407+3602	TV Per	2	0.3	911114	911220
02455+1718	T Ari	1	1.1	911105	···
02455−1240	Z Eri	1	0.7	920113	···
02469+5646	W Per	2	0.5	911113	911220
02473+5738	IRC+60100	2	0.6	911113	···
02532+5426	ER Per	1	0.5	920111	···
02547+1106	02547+1106	2	0.5	911115	···
03030+5532	IO Per	2	0.4	911109	911113
03082+1436	U Ari	1	0.6	911022	920119
03094+5530	03094+5530	1	0.4	920111	···
03113+5441	V 411 Per	2	1.1	911113	···
03170+3150	UZ Per	2	0.3	911114	911220
03206+6521	OH138.0+7.3	3	0.6	911123	920119
03229+4721	V 384 Per	1	0.9	911111	···
03238+6034	03238+6034	1	0.5	920112	920119
03293+6010	AFGL 5097	2	1.0	911106	911109
03385+5927	03385+5927	1	0.3	920111	920119
03415+8010	SS Cep	1	1.1	911111	911112
03448+4432	03448+4432	2	0.4	911113	911220
03489−0131	SU Eri	1	0.6	920113	···
03572+5509	03572+5509	2	0.7	911113	···
04020−1551	V Eri	1	1.1	911029	···
04064+3321	V 394 Per	1	0.8	911106	911109
04137+3114	IRC+30080	1	0.6	920112	···
04260+2437	IRC+20082	1	0.8	911106	911109
04264+0950	S Tau	1	1.3	911023	911030
04265+5718	RV Cam	1	0.5	920111	···
04307+6210	IRC+60144	1	1.2	911111	···
04328+2824	IU Tau	1	0.7	920112	···
04355+0814	RX Tau	1	1.3	911030	920113
04395+3601	AFGL 618	3	0.4	911117	920112
04440+2605	RV Tau	2	0.5	911106	911110
04530+4427	04530+4427	2	0.4	911115	911220
04566+5606	TX Cam	1	0.8	911029	911111
04575+1251	AFGL 5134	2	0.6	911115	···
05073+5248	NV Aur	3	0.7	911023	911116
05090−1154	RX Lep	1	0.9	911111	···
05132+5331	R Aur	1	1.0	911023	911123
05174−3345	T Col	1	1.1	911106	911109
05265−0443	S Ori	1	1.1	911029	911111
05354+2458	05354+2458	1	0.9	911111	···
05361+4644	IRC+50149	3	0.3	911116	920111
05367+3736	RU Aur	1	1.6	911023	911029
05378+2804	05378+2804	1	0.7	920112	···
05384+3854	SZ Aur	1	0.5	920111	···
05418−3224	05418−3224	1	0.9	920119	···
05524+0723	α Ori	1	0.7	911111	···
05543+5002	05543+5002	2	0.6	911115	···
05559+3825	IRC+40419	1	1.3	911111	···
05591+1630	MWC 789	3	1.4	911106	911109
05592−0221	V 352 Ori	1	0.6	911111	···
06003+4747	06003+4747	2	0.7	911115	···
06011+2829	BS Aur	1	0.5	920112	···
06012+0726	06012+0726	2	0.6	911115	···
06027−1628	SS Lep	1	0.7	911112	···
06036−2411	S Lep	1	0.9	911106	911109
06088+2152	TV Gem	1	0.6	920112	···
06092+2255	BU Gem	1	0.6	920112	···
06104+1833	GI Ori	1	0.9	911029	911030
06140−2729	06140−2729	1	1.1	920113	···
06176−1036	HD44179	3	0.4	911117	920113
06181+0406	06181+0406	2	0.5	911115	···
06192+4657	06192+4657	2	0.9	911113	911117
06230−0930	06230−0930	1	0.7	920113	···
06250+6134	06250+6134	2	1.1	911113	911116
06259−1301	FS CMa	2	0.5	911115	911220
06268+0849	06268+0849	1	0.8	920112	···
06297+4045	IRC+40156	2	0.5	911113	911220
06329−0106	06329−0106	2	0.7	911115	···
06333−0520	GL Mon	1	0.8	920113	···
06342+0328	06342+0328	1	0.4	911111	911112
06349−0121	SY Mon	1	0.6	911029	911112
06364+0846	R Mon	3	0.4	911116	920112
06398−0936	06398−0936	2	0.5	911115	···
06402+5757	S Lyn	1	1.2	911030	···
06439+3019	X Gem	1	0.8	911029	911123
06487+0551	AFGL 1020	1	0.6	920113	···

Table 3. (Continued)

IRAS name	Star name	Type	$S \leq$	Obsd1	Obsd2
06491−0654	06491−0654	2	0.5	911115	911220
06496−1858	DL CMa	1	0.8	920113	···
06546−2353	X CMa	1	1.0	920113	···
07021−0852	HN Mon	1	0.8	911111	911112
07098−2012	07098−2012	1	0.7	911111	911112
07150+3808	IRC+40172	1	0.5	911111	911112
07152−3444	AFGL 1099	1	1.2	911106	911109
07153−2411	07153−2411	2	1.3	911115	···
07217−1246	07217−1246	1	0.6	911111	911112
07232−0544	TT Mon	1	1.2	911106	911110
07245+4605	Y Lyn	1	0.7	911111	911112
07266−0541	07266−0541	2	0.3	911114	911115
07299+0825	S CMi	1	0.7	911111	···
07329−2352	07329−2352	2	0.6	911113	911220
07400+2334	S Gem	1	0.9	911106	911110
07418−2850	IRC−30099	1	0.6	911111	911113
07434−3750	BS3017	1	1.2	911112	···
07556−2017	IRC−20152	2	0.5	911113	911220
07582−1933	07582−1933	1	0.6	920113	920119
07585−1242	U Pup	1	0.8	911106	920119
08003+3629	08003+3629	1	0.2	920111	920119
08050−2838	08050−2838	1	1.0	920113	920119
08078−3801	AS Pup	1	1.0	911111	911112
08088−3243	AFGL 1235	1	0.6	911111	911112
08089−3511	08089−3511	2	0.9	911115	···
08138+1152	R Cnc	1	0.6	911111	911123
08149−1339	SV Pup	1	1.1	911106	911110
08171−2134	AFGL 5250	3	0.5	920113	920119
08189+0507	08189+0507	1	0.4	920112	920119
08191−3653	08191−3653	2	1.4	911115	···
08200−2528	08200−2528	2	0.7	911113	911115
08212−3838	08212−3838	1	0.7	920119	···
08272−0609	RT Hya	1	0.6	911111	911112
08340−3357	08340−3357	1	0.8	911111	911112
08372−0924	RV Hya	1	0.9	920113	920119
08375−1707	AK Hya	1	1.1	911111	···
08391+0222	AFGL 1283	2	0.3	911113	911220
08416−2525	IRC−30132	1	0.5	920113	920119
08437+0149	EY Hya	1	0.4	911111	911115
08439−2734	08439−2734	1	0.6	920113	920119
08509+0315	S Hya	1	1.1	911024	911030
08555+1102	RT Cnc	1	0.5	920112	920119
09057+1325	CW Cnc	1	0.3	920112	920119
09076+3110	RS Cnc	1	0.5	911112	911116
09116−2439	09116−2439	1	0.9	911111	···
09429−2148	IW Hya	2	0.8	911106	911220
09448+1139	R Leo	1	1.1	911022	911123
09452+1330	CW Leo	1	0.9	911022	911031
09507+3509	S LMi	1	1.1	911022	911024
09572+2130	V Leo	1	0.7	911106	911110
10131+3049	RW LMi	1	0.8	911105	911112
10353−1145	FF Hya	1	0.8	920112	···
10411+6902	R UMa	1	2.0	911022	···
10491−2059	V Hya	1	1.0	911111	···
11125+7524	CS Dra	1	0.3	920111	920113
11252+1525	AF Leo	2	0.5	911105	911113
11308−1020	11308−1020	1	0.3	920112	920119
11445+4344	11445+4344	2	0.3	911113	911220
11461−3542	HD102608	1	1.0	911111	···
11462−2628	II Hya	1	2.2	911106	911109
11577−0954	SV Vir	1	1.2	911106	911110
12277+0441	BK Vir	1	0.6	911112	···
12359+0715	R Vir	1	1.3	911022	911024
12380+5607	Y UMa	1	1.0	911111	···
12387−3717	12387−3717	2	0.7	911115	···
12449+3838	U Cvn	2	0.6	911022	911105
13068−0927	IRC−10278	1	1.6	911106	911110
13114−0232	SW Vir	1	0.6	911111	911113
13172+4547	V Cvn	1	0.6	911029	911105
13303−0656	S Vir	1	0.9	911105	911111
13336+7341	T UMi	1	0.7	911022	911123
13468+3947	R Cvn	1	0.4	911105	911112
13548−3049	TW Cen	1	1.3	911106	911110
13582+3806	13582+3806	2	0.3	911114	···
14106−2940	14106−2940	1	0.5	920112	920119
14142−1612	EW Vir	1	0.4	920112	920113
14162+6701	U UMi	1	0.3	911105	920111
14251−3246	14251−3246	2	1.0	911115	911116
14280−2952	Y Cen	1	0.9	911112	···
14349+2657	R Boo	1	1.0	911106	911110
14371+3245	RV Boo	1	0.9	911112	···
14390+3147	RW Boo	1	0.4	920112	920119
14550−1214	14550−1214	1	0.4	920112	920113
15214−2244	RS Lib	1	1.1	911023	911123
15223−0203	15223−0203	2	0.4	911115	911220
15262+0400	IRC+00266	2	0.6	911030	911115
15314+7847	S UMi	1	0.9	911022	911029
15341+1515	IRC+20282	1	0.7	911112	···
15402−3700	FQ Lup	1	0.7	920119	···
15483+1517	R Ser	1	0.4	911030	911115
15492+4837	ST Her	1	0.6	911112	···
15589−2850	15589−2850	1	1.3	920113	···
16015−2357	RZ Sco	1	1.8	911109	911111
16081+2511	RU Her	1	0.8	911106	911110
16146−2246	S Sco	1	1.8	911109	···
16211+3057	RY Crb	1	0.6	911108	911111
16260+3454	V 697 Her	2	0.4	911022	911220
16308−1601	T Oph	1	1.0	911030	911123
16325+6651	R Dra	1	0.6	911106	911123
16334−3107	ST Sco	1	1.0	920113	···
16418+5459	S Dra	1	0.8	911112	···
16438−1133	V 446 Oph	1	1.0	911112	···
16473+5753	AH Dra	1	0.4	920111	920113
16494−1252	IRC−10348	1	0.8	920113	···
16521−2153	SY Oph	1	0.8	920113	···
16534−3030	RR Sco	1	0.9	911106	911112
16560+2252	MV Her	1	0.7	911029	911123
17050+1714	VY Her	1	1.0	911029	911123
17079−3243	17079−3243	1	1.3	911112	911113
17081+6422	TV Dra	1	0.5	920111	920113

Table 3. (Continued)

IRAS name	Star name	Type	$S \leq$	Obsd1	Obsd2
17102−1031	IRC−10359	2	0.7	911115	···
17123+1107	V 438 Oph	1	0.4	911107	920112
17150−1156	RV Ser	1	0.9	911107	911111
17171−0843	17171−0843	2	0.8	911115	···
17187−3750	17187−3750	2	2.8	911111	···
17256+0504	IRC+10329	2	1.1	911030	911106
17265−0725	IRC−10369	1	0.7	911113	···
17297+1747	IRC+20326	2	0.5	911114	911220
17309−1724	AFGL 5353	2	1.4	911030	···
17313−1531	17313−1531	2	1.4	911115	···
17334+1537	MW Her	2	0.5	911114	911220
17361+5746	TY Dra	2	0.5	911113	911220
17485−2209	IRC−20394	1	0.9	920113	···
17504−0234	17504−0234	1	0.5	920113	···
17507−1122	17507−1122	2	0.9	911115	···
17528+1144	17528+1144	2	0.6	911106	911107
17528−1503	OH13.1+5.1	3	1.7	911109	···
17541+1110	RT Oph	1	0.7	911022	920112
17570−3713	17570−3713	1	1.2	911112	···
17594+0826	17594+0826	1	1.0	911107	···
17599−3653	17599−3653	1	1.4	911112	···
18009−1539	18009−1539	2	1.0	911118	···
18069+0911	18069+0911	2	0.6	911106	911114
18072+3100	T Her	1	0.7	911022	911029
18076+3445	18076+3445	2	0.5	911022	911117
18083−2630	AFGL 2086	2	0.7	911105	···
18092−0437	18092−0437	2	1.0	911118	···
18112+1227	V 454 Oph	2	1.1	911114	···
18156−0653	18156−0653	1	0.7	911112	···
18184−1302	18184−1302	3	0.7	911118	920113
18231+0855	18231+0855	2	0.8	911106	911107
18238−2542	HO Sgr	1	0.7	920119	···
18240+2326	AFGL 2155	1	0.9	911113	···
18248−0839	18248−0839	2	1.1	911114	···
18257−1000	V 441 Sct	3	1.4	911109	···
18266−1239	V 435 Sct	3	1.2	911109	···
18270+0326	18270+0326	2	1.5	911107	···
18276+8236	18276+8236	2	0.6	911113	911116
18276−1431	OH17.7−2.0	3	1.5	911109	···
18298−2111	18298−2111	3	0.9	920114	···
18304−0728	IRC−10434	2	1.2	911114	···
18314−1131	18314−1131	1	0.8	911112	···
18325−1138	18325−1138	2	2.1	911114	···
18333+0533	18333+0533	2	0.6	920119	···
18344−0850	OH23.5−0.9	2	1.5	911109	···
18359+0847	X Oph	1	1.2	911022	911029
18373−0021	AFGL 2222	2	0.6	911116	···
18375+0510	18375+0510	2	0.9	911106	911107
18398−0220	18398−0220	1	1.0	911112	···
18414−0527	18414−0527	2	1.3	911114	···
18437−0643	V 440 Sct	3	1.1	911109	···
18450−0922	18450−0922	2	1.5	911114	···
18451−0824	18451−0824	2	1.5	911114	···
18465−0717	18465−0717	2	0.6	911127	···
18475+0926	AFGL 2259	1	0.7	911112	···
18476−0758	S Sct	1	0.8	911105	···
18476+0555	18476+0555	2	1.6	911114	···
18487+0152	OH34.7+0.9	3	1.7	911109	···
18501−2132	V 2059 Sgr	1	0.5	911109	···
18512−0934	18512−0934	2	1.3	911114	···
18512+2029	18512+2029	2	1.5	911116	···
18520−1635	UX Sgr	1	0.8	920114	···
18520+1014	18520+1014	2	0.8	911106	911107
18522+0021	IRC+00392	2	1.4	911114	···
18526+0140	18526+0140	3	0.7	911116	920119
18530+0817	18530+0817	2	1.2	911114	···
18535+0726	OH40.1+2.4	2	0.6	911107	911123
18540+0302	18540+0302	3	1.3	911109	···
18545+1040	18545+1040	2	1.4	911114	···
18549+0905	18549+0905	2	1.0	911107	···
18556+0811	18556+0811	2	0.8	911107	911114
18560−2954	V 3953 Sgr	1	1.2	911112	···
18562−0303	EU Aql	2	1.6	911109	···
18567+0003	18567+0003	2	1.0	911109	911114
18592+1455	18592+1455	2	1.1	911116	···
19008+0726	IRC+10401	1	0.8	911112	···
19029+2017	AFGL 2318	1	0.6	920111	···
19043+1009	19043+1009	2	1.0	911116	···
19047−1706	FQ Sgr	1	1.1	911109	920114
19055+0613	19055+0613	1	0.8	920114	···
19059−2219	V 3880 Sgr	2	1.4	911109	···
19067+0811	V 1368 Aql	3	0.5	911107	911123
19071+0946	OH43.8+0.5	3	0.7	911107	911123
19087+0323	19087+0323	2	1.5	911107	···
19093−3256	V 342 Sgr	2	1.1	911116	···
19099+6711	U Dra	1	0.5	911022	911105
19107+4113	RU Lyr	1	0.8	911022	911105
19126−0708	W Aql	1	0.6	911112	···
19134+2131	19134+2131	3	1.0	911106	911109
19135+0931	AFGL 2350	2	1.4	911114	···
19160+0755	19160+0755	3	1.2	911107	···
19161+2343	AFGL 2362	2	0.7	911106	920113
19186+0315	19186+0315	2	1.1	911107	···
19192+0922	OH44.79−2.313	0.7	911107	920113	
19194+1734	T Sge	1	0.9	911112	···
19231+3555	IRC+40346	2	1.1	911117	···
19240+3615	19240+3615	2	0.8	911117	···
19244+1115	19244+1115	3	0.4	911117	920112
19248+0658	19248+0658	1	0.6	920113	···
19267+0345	19267+0345	2	1.0	911114	···
19270+2239	19270+2239	2	0.7	911116	···
19283+1944	OH55.0+0.7	3	0.4	911117	920111
19288+2923	OH63.5+5.3	2	0.7	911106	911109
19303+1553	19303+1553	2	1.1	911107	···
19321+2757	19321+2757	1	0.9	911112	···
19328+3039	19328+3039	1	1.0	920119	···
19329+2641	19329+2641	2	0.7	911116	···
19334−0033	V 1319 Aql	1	1.3	911107	···
19348+2136	IRC+20419	2	0.9	911114	···
19352+2030	OH56.4−0.3(?)	3	1.5	920111	···

Table 3. (Continued)

IRAS name	Star name	Type	$S \leq$	Obsd1	Obsd2
19371+2855	19371+2855	2	0.6	911117	···
19386+1513	OH52.2−3.6	2	0.7	911107	911116
19455+0920	19455+0920	1	0.5	920112	···
19456+1927	19456+1927	2	0.8	911106	911123
19467+2213	OH59.2−1.8	2	1.2	911107	···
19474−0744	GY Aql	1	0.9	911112	···
19480+2447	NR Vul	1	0.8	911112	···
19486+3247	X Cyg	1	0.6	911022	911105
19493+2905	OH65.4+1.3	2	1.1	911106	911109
19499+2141	19499+2141	2	1.6	911107	···
19503+2219	NS Vul	1	0.8	911112	···
19508+2659	OH63.9−0.2	2	1.0	911106	911107
19522+1935	19522+1935	2	1.2	911107	···
19528−2919	RR Sgr	1	1.2	911105	911112
19528+0148	19528+0148	2	0.8	911114	···
19552+3142	19552+3142	2	1.0	911116	···
19585+5200	19585+5200	1	0.6	920112	···
19586+3637	V 1511 Cyg	2	0.8	911113	···
19591+1817	19591+1817	2	0.4	911116	···
19594+4047	19594+4047	2	0.9	911113	···
20000+4954	Z Cyg	2	1.9	911022	911116
20010+3011	20010+3011	2	1.0	911113	···
20024+1727	20024+1727	2	0.5	911116	···
20052+0554	IRC+10451	2	0.8	911114	···
20077−0625	V 1300 Aql	2	0.5	911116	···
20079−0146	V 584 Aql	1	0.4	920112	···
20082+3228	20082+3228	1	0.7	920112	···
20097+1107	20097+1107	2	1.3	911107	···
20113+4917	AC Cyg	1	0.5	911106	920112
20171+2732	20171+2732	2	1.0	911022	911030
20171+3519	20171+3519	2	0.8	911113	···
20194+3646	BI Cyg	2	0.8	911106	911107
20215+3205	20215+3205	2	0.8	911113	···
20217+3330	20217+3330	2	0.7	911113	···
20233+3343	20233+3343	2	0.8	911113	···
20234−1357	20234−1357	2	0.8	911116	···
20246+2813	20246+2813	2	1.3	911022	···
20248−2825	T Mic	1	1.7	911112	···
20248+7505	UU Dra	2	0.8	911115	···
20311+4222	20311+4222	1	0.5	911112	911113
20331+4621	20331+4621	1	0.5	920119	···
20350+3741	V 1828 Cyg	1	0.6	920113	···
20350+5954	V 778 Cyg	1	0.7	911106	911109
20365+1154	20365+1154	2	0.9	911114	···
20377+3901	IRC+40439	2	0.9	911113	···
20381+5001	20381+5001	2	0.6	911114	···
20403+3143	20403+3143	2	0.9	911109	···
20403+3700	20403+3700	2	0.7	911113	···
20431+1754	U Del	1	0.8	911112	···
20435+3825	20435+3825	1	0.6	911112	911113
20440−0105	FP Aql	1	0.9	911112	911113
20443+0215	V Aqr	1	1.0	911109	···
20444+0540	20444+0540	2	0.7	911114	···
20467−0044	20467−0044	1	0.7	920112	···
20482+3325	20482+3325	2	0.8	911107	911109
20502+4709	RZ Cyg	1	0.6	911112	911113
20507+2310	RX Vul	1	0.5	920112	···
20532+5554	20532+5554	2	0.8	911113	···
20547+0247	U Equ	2	1.2	911109	···
20570+2714	AFGL 2686	1	1.2	911112	···
21003+4801	21003+4801	2	0.9	911113	···
21006+4720	21006+4720	1	0.7	920113	···
21027+3704	GR Cyg	1	0.6	920119	···
21027+5309	21027+5309	2	0.8	911113	···
21029+4917	21029+4917	2	0.9	911106	···
21032−0024	RV Aqr	1	0.6	911112	···
21035+5136	V 1549 Cyg	1	0.5	911112	911113
21044−1637	RS Cap	1	1.0	911113	···
21120+0736	21120+0736	2	0.5	911109	911114
21147+5110	21147+5110	2	1.2	911113	···
21174+1747	21174+1747	2	1.4	911109	···
21208+7737	GH Cep	1	0.8	920111	···
21245+6221	SW Cep	2	0.5	911114	···
21270+7135	21270+7135	1	0.8	911112	911113
21282+5050	21282+5050	3	0.6	920113	···
21286+1055	UU Peg	2	0.6	911109	911114
21305+2118	21305+2118	2	1.0	911114	···
21312+5405	IRC+50583	1	0.9	920113	···
21318+5631	21318+5631	3	0.3	911116	920113
21320+3850	V 1426 Cyg	1	0.7	911112	···
21324+5537	21324+5537	2	0.9	911113	···
21341+4508	W Cyg	1	0.6	911112	911113
21345+5410	21345+5410	2	0.9	911113	···
21373+4540	21373+4540	1	0.5	911112	911113
21377−0200	21377−0200	1	0.5	920112	···
21389+5405	RU Cyg	1	0.7	911113	···
21414+7609	AM Cep	1	1.0	911107	911109
21419+5832	μ Cep	1	0.9	911105	911111
21449+4950	21449+4950	2	1.2	911113	···
21456+6422	21456+6422	1	0.8	911111	911113
21468+3942	IRC+40497	2	0.7	911117	···
21543−1421	IRC−10573	1	0.4	920112	···
21554+6204	21554+6204	3	0.4	911116	920111
21565+4132	21565+4132	1	0.6	920113	···
21585+0552	V Peg	1	1.9	911030	···
22017+2806	TW Peg	1	0.6	911022	911112
22097+5647	CU Cep	2	0.7	911106	911109
22177+5936	OH104.91+2.43	1	0.5	911022	920111
22190−0751	22190−0751	1	0.8	920112	···
22233+3013	RV Peg	1	1.0	911030	911112
22241+6005	22241+6005	1	0.7	911111	911113
22264+5858	22264+5858	1	0.6	920112	···
22277+4534	IRC+50434	1	0.9	911106	911107
22282+5644	ST Cep	2	1.0	911113	···
22315+2418	SS Peg	1	1.3	911022	···
22317+5838	V 354 Cep	1	0.6	920112	···
22345+5809	W Cep	2	0.9	911113	···
22402+1045	22402+1045	2	0.6	911109	···
22413+5929	IRC+60364	1	0.6	920111	···
22456+5453	U Lac	1	0.8	911111	911113

Table 3. (Continued)

IRAS name	Star name	Type	$S \leq$	Obsd1	Obsd2
22525−2952	V Psa	1	1.3	911113	···
22546+6115	IRC+60377	2	1.0	911113	···
22594+6117	22594+6117	2	1.2	911113	···
23000+5932	23000+5932	2	0.7	911113	···
23138+6204	IRC+60393	2	0.7	911113	···
23166+1655	23166+1655	3	0.6	911117	911125
23173+2600	W Peg	1	0.7	911022	911112
23176+4658	EU And	2	1.9	911107	911123
23180+0838	S Peg	1	0.6	911105	···
23212+3927	BU And	1	0.7	911030	911111
23257+1038	AFGL 3099	2	0.8	911115	···
23278+6000	V 582 Cas	2	1.0	911113	···
23279+5336	23279+5336	1	1.3	920112	···
23281+5742	V 358 Cas	2	0.8	911113	···
23284+5958	23284+5958	2	0.8	911113	···
23312+0601	IRC+10537	1	0.9	911105	···
23320+4316	LP And	1	1.0	911022	911030
23365+5159	SV Cas	2	1.2	911111	···
23412−1533	R Aqr	1	0.8	911105	···
23420+5618	Z Cas	1	0.4	920111	···
23425+4338	EY And	2	1.1	911022	911115
23496+6131	V 657 Cas	2	0.8	911022	911113
23504+6043	TZ Cas	2	0.8	911113	···
23528+4821	RS And	1	0.8	911030	911111
23575+2536	Z Peg	1	0.7	920113	···

typical one for dust-enshrouded AGB stars with SiO masers (Izumiura et al. 1995).

In order to investigate the dependence of the detection rate on the IRAS properties more carefully, we calculated the luminosity distances from the Sun for each type of source and plotted the histograms and detection rates in figure 3b. Here the luminosity distances are computed from the IRAS 12 μm flux density and the color C_{12} (van der Veen, Breuckers 1989); see the prescription in Jiang et al. (1996), or Deguchi et al. (1999). We assumed a constant luminosity, 8000 $L_\odot$, for all the sources. This luminosity is probably somewhat too large for Type-1 sources (optically seen Mira and semiregular variables). Figure 3b shows histograms of the luminosity distances for three types of sources. They show a decreasing tendency of the detection rate with distance as a whole, although some artifact due to a small number of samples is seen at large distances in the second panel (Type 2). It can be seen that the Type-1 sources are systematically closer than the Type-2 sources; the average distance is 0.71 (±0.48) kpc for the Type-1 H_2O detected sources, whereas it is 1.4 (±1.2) kpc for Type-2 detected sources (here, the number in parentheses is the standard deviation). Considering that the luminosities for these optically seen variables are slightly smaller than the assumed 8000 $L_\odot$ used in the distance calculation, the real distances for the Type-1 sources may be a factor of 1.5 smaller than the above calculated distances. Thus, the low detection rate of the Type-2 sources is explained by their larger distances.

The average distance for the H_2O-detected Type-3 sources, 3.6 (±3.0) kpc, is larger than that for the Type-2 sources. It seems that the detection rate for the Type-3 sources exceeds that for the Type-2 sources. We also calculated the intrinsic power (D^2S) of H_2O masers corrected for the distance. The average power for the Type-3 sources is 82 (±135) Jy (kpc)^2, whereas the powers for the Type-1 and -2 sources are 4.9 (±8.1) and 17 (±23) Jy (kpc)^2, respectively. Though the standard deviations for these averages are very large, the Type-3 sources have larger intrinsic maser power on average. Therefore, the high detection rate for the Type-3 sources are probably attributed to their high maser power.

It is possible, however, that the distances to these sources with a cold dust envelope can not be computed with reasonable accuracy from the IRAS 12 μm flux density and the color C_{12}. The type-3 sample involves 5 very distant ($D > 8$ kpc) sources: 05591+1630, 18056−1954, 18596+0315, 19069+0916, and 19134+1630; 3 of these 5 sources were detected in H_2O. The distance of 18596+0315 (OH 37.1−0.8) was estimated as 9.9 kpc in this paper. The color of this source is (C_{12}, C_{23}) = (0.74, 0.20), indicating that this is a source with a detached shell (Lewis, te Lintel-Hekkert 1991). The double peaks of the OH 1612 MHz line (Baud et al. 1985) and of the main lines (Lewis 1997b) were observed at V_{lsr} = 75 and 101 km s^{-1}; the H_2O velocity at V_{lsr} = 65.6 km s^{-1} is slightly lower than the lower velocity of the OH peaks, but is consistent with the previous H_2O observation (Engels et al. 1986). The SiO J = 1–0, v = 1 maser was detected by Jewell et al. (1991), but the J = 2–1, v = 2 line searches were negative (Nyman et al. 1993, 1998). Based on the near-IR photometry, Sun and Zhang (1998) estimated the distance to this star as being 5.3 kpc, which is slightly less than the value given in the present paper.

3.2. *Velocity Spread of the* H_2O *Spectra*

We have plotted the line width, ΔV, against the colors in figure 4. Several sources have a very large ΔV above 25 km s^{-1} (see the definition of the ΔV for double-peak and multiple-peak sources in section 2); these are 17501−2656, 18327−0715, 19069+0916, and 19083+0851. The H_2O maser at 22 GHz has already been detected for all of these sources; Engels and Lewis (1996) observed the H_2O emission from V_{lsr} = 28.6 to 72.9 km s^{-1} for 19083+0851, and from V_{lsr} = 11.2–43.8 km s^{-1} for 19069+0916, and Engels et al. (1986) detected double peaks centered at −6 km s^{-1} for 17501−2656 (OH 2.58−0.43), being consistent with the present result. For 18327−0715 (OH 24.7+0.2), Gomez et al. (1990) detected a broad H_2O feature spreading in V_{lsr} = 25–35 km s^{-1} and SiO maser emission in V_{lsr} = 43.3 and 47.5 km s^{-1}. We have detected another component spreading 55–58 km s^{-1}, consistent with the double peaks of H_2O masers centered at V_{lsr} = 41 km s^{-1}, and with the middle velocity of OH 1612 MHz emission at V_{lsr} = 42 km s^{-1} (te Lintel-Hekkert et al. 1989).

Figure 4 seems to show a tendency that the velocity spread in the double- or multiple-peak sources increases with the IRAS color untill $C_{12} \sim 0.0$. Though 4 sources on the right side of the panels (beyound C_{12} = 0.5) do not follow this tendency,

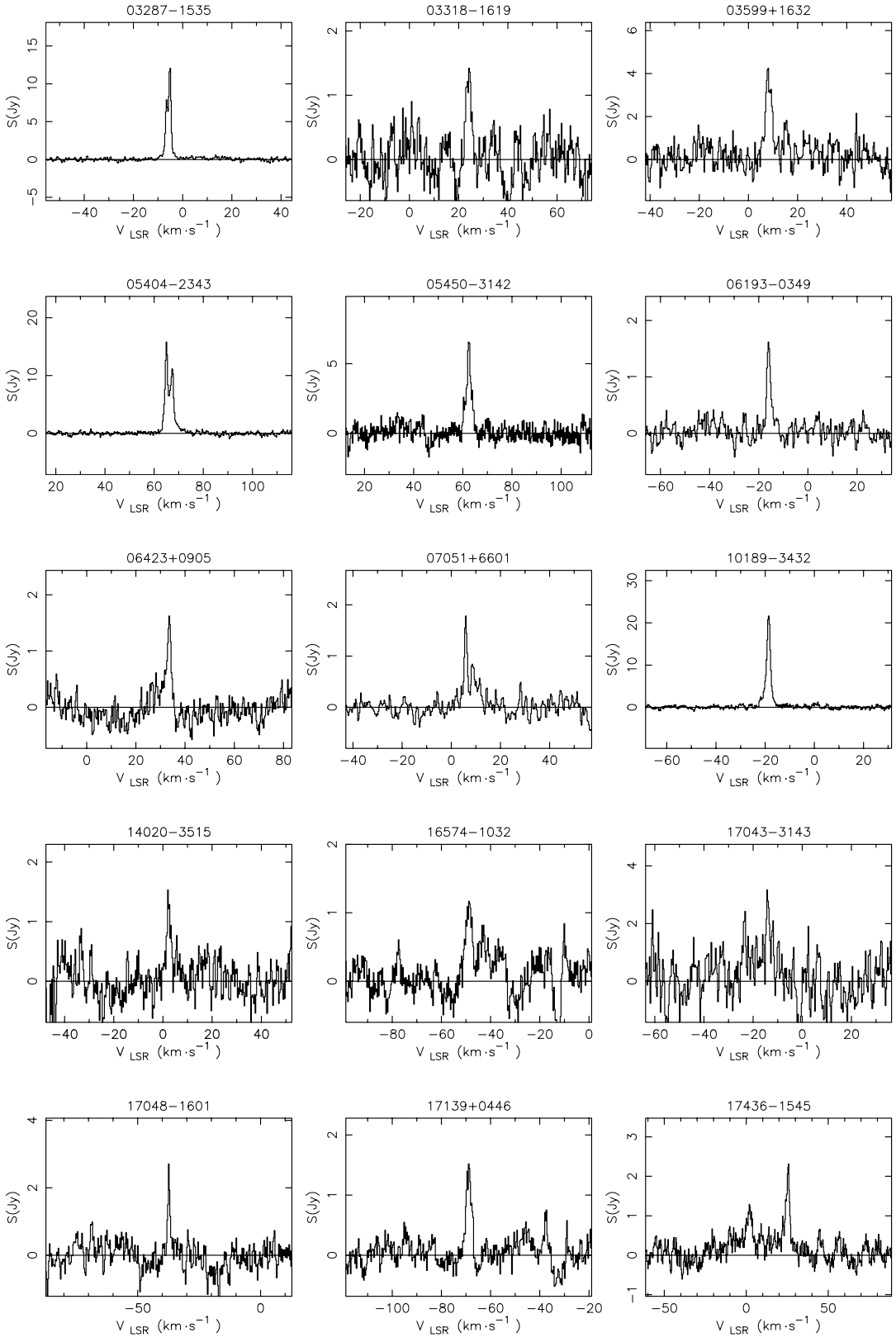

Fig. 2a. Water maser spectra of 32 new detections plus a few interesting known detections.

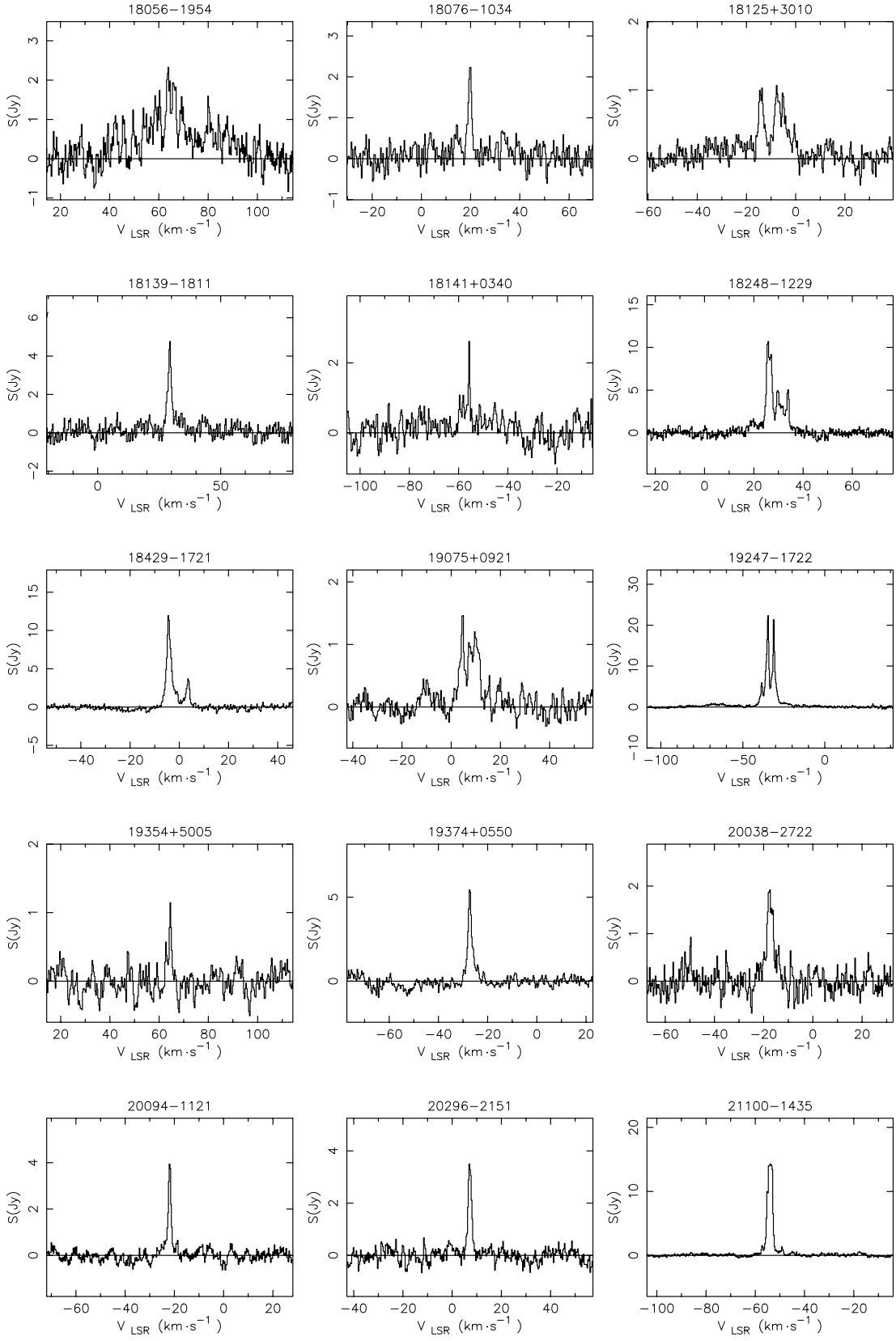

Fig. 2b. Water maser spectra of 33 new detections.

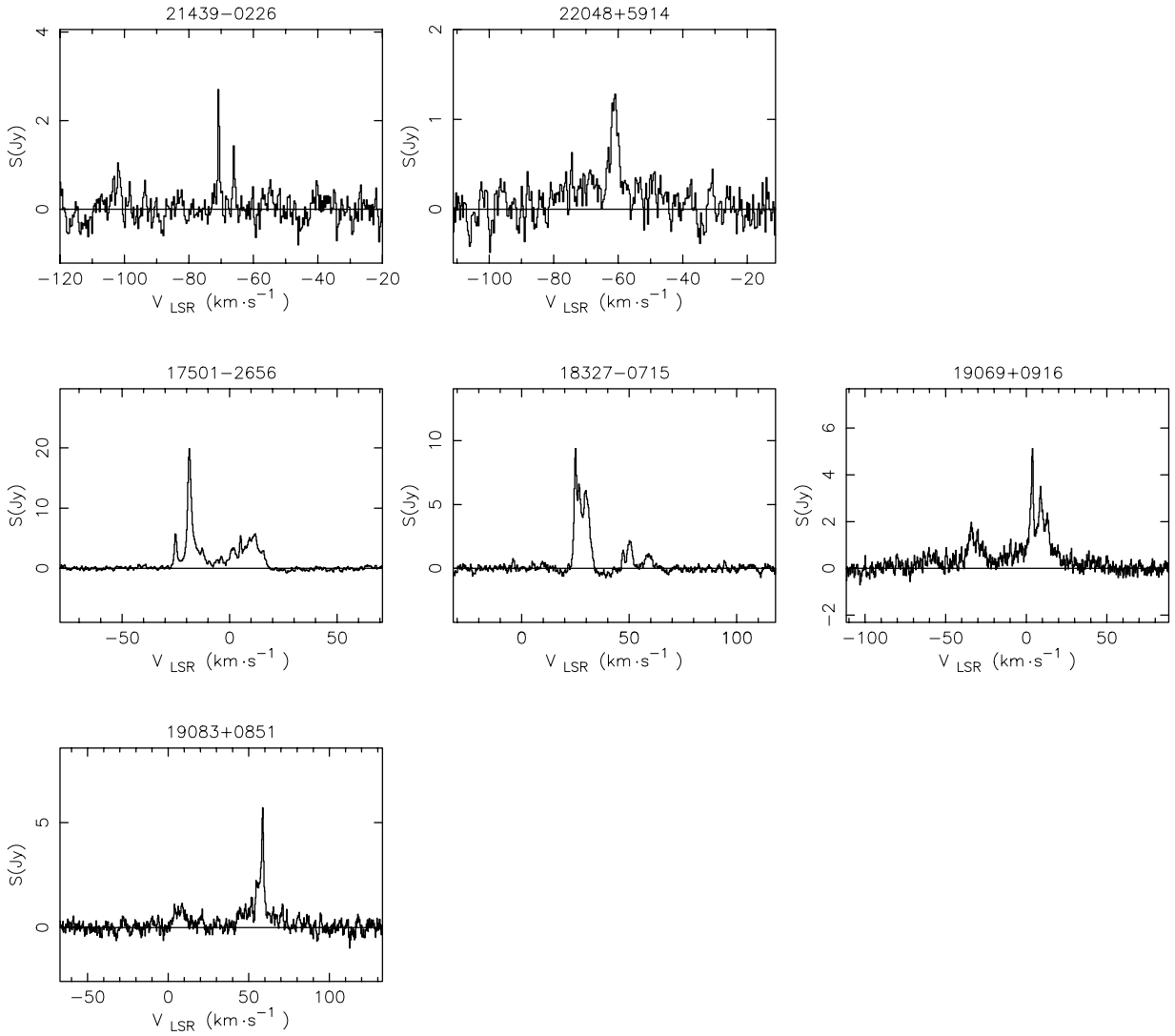

Fig. 2c. Water maser spectra of 33 new detections.

this is, however, an artifact. These sources are well known protoplanetary-type OH/IR sources with a large line spread in OH 1612 MHz: 07399−1439 (OH 231.8+4.2 or QX Pup), 18056−1954 (OH 10.4+0.04), 18596+0315 (OH 37.1−0.8) and 19110+1045 (OH 45.07+0.13). In these sources, the intensity of the lower velocity component in the double peaks tends to surpass the intensity of the higher velocity component (see Takaba et al. 1994). Therefore, weaker components in the H_2O profle were often missed in the present survey because of the telecope sensitivity. For example, Engels and Lewis (1996) detected the wearker component of 0.3 Jy at $V_{\rm lsr} = 112.9\,{\rm km\,s^{-1}}$ in 18596+0315, whereas the present paper gives only the strongest component at $65.6\,{\rm km\,s^{-1}}$ (table 2). The color, $C_{12} \sim 0.5$, corresponds to the limit of the SiO maser detection (Nyman et al. 1998). This color corresponds to an edge of the transition of the (oxygen-rich) Asymptotic Giant Branch stars to protoplanetary nebulae in the two-color diagram, where the mass-loss rate of the central star suddenly decreases after the final He-shell flash (Vassiliadis, Wood 1993). The numerical modeling of the transient envelopes of post-AGB stars (van Hoof et al. 1997) confirmed that the transition occurs near this color.

It is well known that the radial velocity of most of SiO maser lines coincides with the stellar velocity, i.e., the middle velocity of the OH 1612 MHz double peaks (Jewell et al. 1991). The H_2O maser spectra, however, often exhibit double peaks with slightly higher and lower radial velocities to the stellar velocity (with stronger "blue-shifted" peak; Takaba et al. 1994), or a single peak at the stellar velocity (Engels et al. 1986). Stars with lower mass-loss rate tend to show the single peak at the stellar velocity, indicating that the maser emission of this type is tangentially beamed (Deguchi 1977). The H_2O masers are considered to be emitted at a few stellar radii of the central star, slightly outside of the SiO maser emitting region, implying that direction of the maser beaming (radial or tangential) changes with the mass loss rate; as the mass-loss rate increases, the

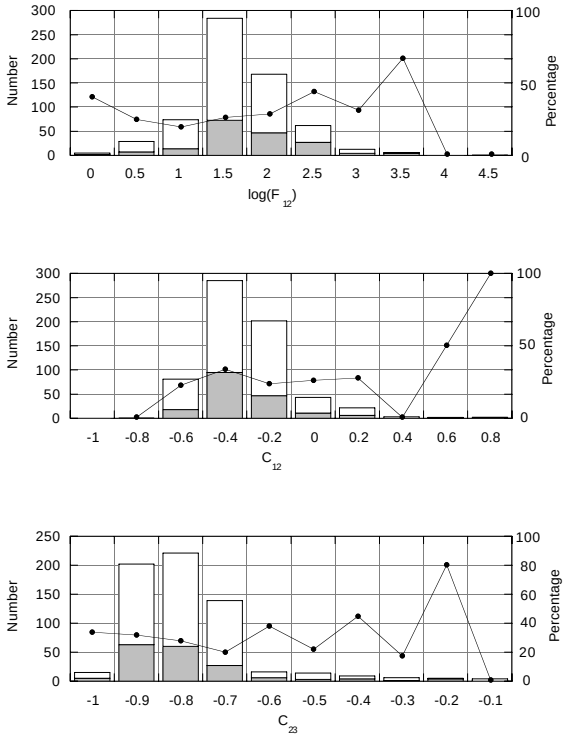

Fig. 3a. Histograms of the IRAS 12 μm flux density (upper panel), the colors C_{12} (middle panel) and C_{23} (lower panel). The line graph shows the detection rate and the scale is shown on the right axis.

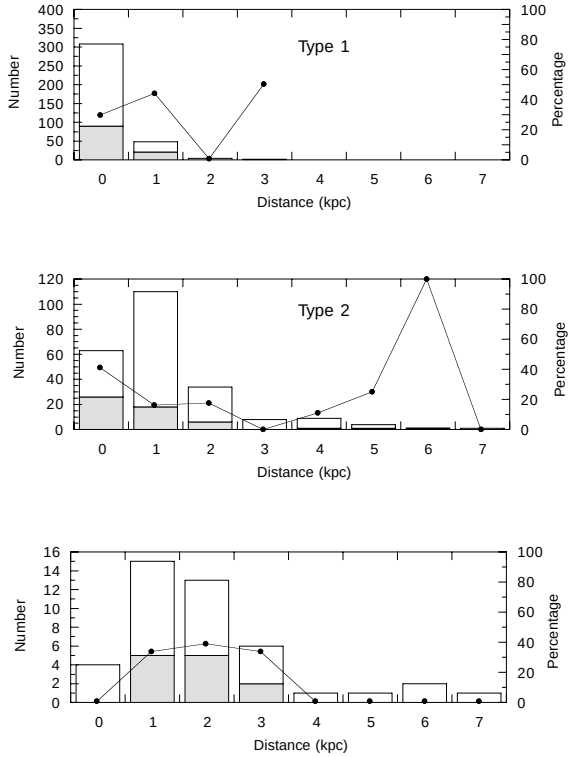

Fig. 3b. The histograms of the luminosity distances for the three types of sources. The average distance increases with the type.

maser emitting region is placed at the outer radii where the acceleration becomes negligible. (see Deguchi 1977).

3.3. Galactic Distribution of Sources

The observed source positions are plotted in the galactic coordinates in the upper panel of figure 5. The sources are missing in the lower-left and lower-right parts of the upper panel because a part of the sky ($\delta < -40^\circ$) is not observable at Kashima. Although the sources are somewhat concentrated near the galactic plane ($l \sim 0^\circ$), approximately half of the detected sources are above $|b| = 10^\circ$, indicating that most of the sources are near to the Sun. In addition, the observed radial velocities of the detected sources are plotted against the galactic longitude in the lower panel of figure 5. The expected radial velocity due to galactic rotation (at the distance of 3 kpc) is shown by the solid curve. The plotted positions of the sources in this diagram do not seem to follow the Galactic rotation but, rather, they spread randomly in velocity, indicating that most of the detected sources are in the proximity of the Sun. This fact is consistent with the short distances of the sampled stars that were obtained in subsection 3.1.

We must note that the radial velocity of the H_2O maser line does not necessarily represent the stellar velocity, as discussed in subsection 3.2. However, the shift of the radial velocity is mostly less than 10 km s^{-1} from the stellar velocity, except a few OH/IR sources having velocity spreads of more than 25 km s^{-1}. The main conclusion that these sources are in the proximity of the Sun does not change due to this relatively minor shift of the H_2O radial velocity.

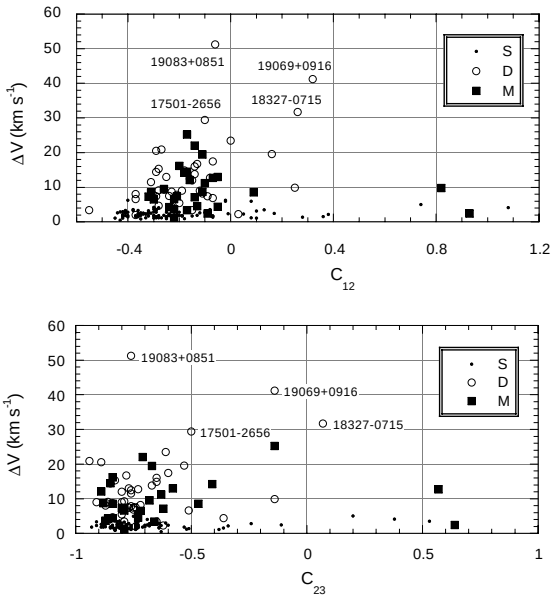

Fig. 4. Plots of the velocity spread against the IRAS colors, C_{12} (upper panel), and C_{23} (lower panel).

4. Summary

We have detected 179 out of 643 observed sources in the 22 GHz H_2O line, including 32 new detections. The luminosity distances were calculated from the IRAS 12 μm flux den-

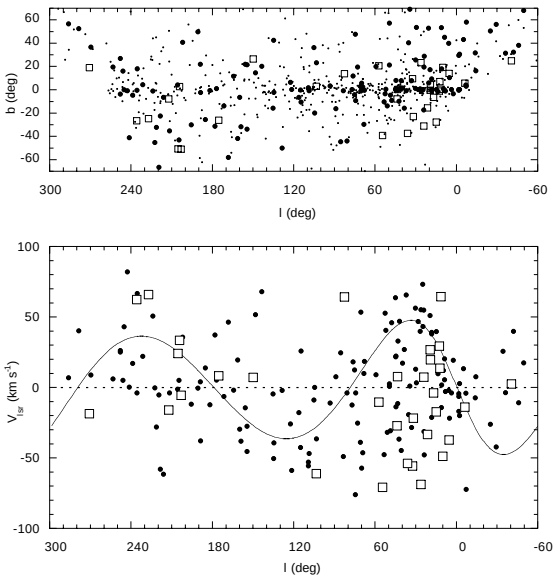

Fig. 5. The upper panel is a plot of the source positions in the Galactic coordinates, and the lower panel a longitude–velocity diagram, for the new (squares), known (filled circles), and non (dot) detections.

sity and the color C_{12}; results show that most of the detected sources are in the proximity of the Sun, within 2 kpc, except for a few OH/IR sources. The longitude–velocity diagram of the detected sources also agrees with the above results. The velocity spread of the H_2O profile has a tendancy to increase with the color.

The authors thank Drs. N. Ukita and M. Miyoshi for discussions. They also thank the staff of Kashima Space Research center for the help to use the 34-m antenna. This research made use of SIMBAD database, operated at CDS, Strasbourg, France.

References

Aoki, W., & Tsuji, T. 1997, A&A, 328, 175
Barvainis, R., & Deguchi, S. 1989, AJ, 97, 1089
Baud, B., Habing, H. J., Matthews, H. E., & Winnberg, A. 1979, A&AS, 36, 193
Baud, B., Sargent, A. I., Werner, M. W., Bentley, A. F. 1985, ApJ, 292, 628
Benson, P. J., Little-Marenin, I. R., Woods, T. C., Attridge, J. M., Blais, K. A., Rudolph, D. B., Rubiera, M. E., & Keefe, H. L. 1990, ApJS, 74, 911
Benson, P. J., & Little-Marenin, I. R. 1996, ApJS, 106, 579
Bowers, P. F., & Hagen, W. 1984, ApJ, 285, 637
Brand, J. Cesaroni, R., Caselli, P., Catarzi, M., Codella, C., Comoretto, G., Curioni, G. P., Curioni, P., di Franco, et al. 1994, A&AS, 103, 541 (and see the updated catalog in ⟨http://www.arcetri.astro.it/science/Radio/cat/cat.html⟩)
Bujarrabal, V., Alcolea, J., Sánchez, C. C., & Colomer, F. 1996, A&A, 314, 883
Cami, J., Yamamura, I., de Jong, T., Tielens, A. G. G. M., Justtanont, K., & Waters, L. B. F. M. 2000, A&A, 360, 562
Cesaroni, R., Palagi, F., Felli, M., Catarzi, M., Comoretto, G., Di Franco, S., Giovanardi C., & Palla, F. 1988, A&AS, 76, 445
Deguchi, S. 1977, PASJ, 29, 669
Deguchi, S., Fujii, T. Izumiura, H., Matsumoto, S., Nakada, Y., Wood, P. R., & Yamamura, I. 1999, PASJ, 51, 355
Deguchi, S., Nakada, Y., & Forster, J. R. 1989, MNRAS, 239, 825
Deguchi, S., Nakashima, J., & Balasubramanyam, R. 2001, PASJ, 53, 305
Engels, D., & Lewis, B. M. 1996, A&AS, 116, 117
Engels, D., Schmid-Burgk, J., & Walmsley, C. M. 1986, A&A, 167, 129
Genzel, R., & Downes, D. 1977, A&AS, 30, 145
Gomez, Y., Moran, J. M., & Rodriguez, L. F. 1990, Rev. Mex. Astron. Astrofis. 20, 55
Groenewegen, M. A. T., & de Jong, T. 1998, A&A, 337, 797
Haikala, L. K. 1990, A&AS, 85, 875
Haikala, L. K., Nyman L.-Å., & Forsström V. 1994, A&AS, 103, 107
Hall, P. J., Allen, D. A., Troup, E. R., Wark, R. M., & Wright, A. E. 1990a, MNRAS, 243, 480
Hall, P. J., Wright, A. E., Troup, E. R., Wark, R. M., & Allen, D. A. 1990b, MNRAS, 247, 549
Han, F., Mao, R. Q., Lu J., Wu, Y. F., Sun, J., Wang, J. S., Pei, C. C., Fan, Y., Tang, G. S., & Ji, H. R. 1998, A&AS, 127, 181
Izumiura, H., Deguchi, S., Hashimoto, O., Nakada, Y., Onaka, T., Ono T., Ukita, N., & Yamamura, I. 1995, ApJ, 453, 837
Jewell, P. R., Snyder, L. E., Walmsley, C. M., Wilson, T.L., & Gensheimer, P. D. 1991, A&A, 242, 211
Jiang, B. W., Deguchi, S., & Nakada, Y. 1996, AJ, 111, 231
Le Squeren, A. M., Sivagnanam, P., Dennefeld, M., & David, P. 1992, A&A, 254, 133
Lewis, B. M., & te Lintel-Hekkert, P. 1991, Proc. Astron. Soc. Australia, 9, 304
Lewis, B. M., David, P., & Le Squeren, A. M. 1995, A&AS, 11, 237
Lewis, B. M. 1997a, AJ, 114, 1602
Lewis, B. M. 1997b, ApJS, 109, 489
Meixner, M., Ueta, T., Dayal, A., Hora, J. L., Fazio, G., Hrivnak, B. J., Skinner, C. J., Hoffmann, W. F., & Deutsch, L. K. 1999, ApJS, 122, 221
Nyman, L.-Å., Booth, R. S., Carlström, U., Habing, H. J., Heske, A., Sahai, R., Stark, R., van der Veen, W. E. J. C., & Winnberg, A. 1992, A&ApS 93, 121
Nyman, L.-Å., Hall, P.J., & Le Bertre, T. 1993, A&A, 280, 551
Nyman, L.-Å., Hall, P.J., & Oloffson, H. 1998, A&AS, 127, 185
Reid, M. J., & Moran, J. M. 1981, ARA&A, 19, 231
Sivagnanam, P., Le Squeren, A. M., Foy, F., & Tran Minh, F. 1989, A&A, 211, 341
Skrutskie, M. F., Stiening, R., Cutri, R., Beichman, C., Capps, R., Carpenter, J., Chester, J., Elias, J. et al. 2000 (The 2MASS Team) ⟨http://www.ipac.caltech.edu/2mass/overview/2massteam.html⟩

Stephenson, C. B. 1990, AJ, 100, 569
Sun, J., & Zhang, H.-Y. 1998, Chinese Astron. Astrophys., 22, 442
Szymczak, M., & Engels, D. 1995, A&A, 296, 727
Szymczak, M., & Engels, D. 1997, A&A, 322, 159
Takaba, H. 1991, J. Comm. Res. Lab., 38, 417
Takaba, H., Ukita, N., Miyaji, T., & Miyoshi, M. 1994, PASJ, 46, 629
te Lintel Hekkert, P., Versteege-Hensel, H. A., Habing, H. J., & Wiertz, M. 1989, A&AS, 78, 399
te Lintel Hekkert, P., Caswell, J. L., Habing, H. J., Haynes, R. F., & Norris, R. P. 1991, A&AS, 90, 327
van der Veen, W. E. C. J., & Breukers, R. J. L. H. 1989, A&A, 213, 133
van der Veen, W. E. C. J., & Habing, H. J. 1988, A&AS, 194, 125
van Hoof, P .A. M., Oudmaijer, R. D., & Waters, L. B. F. M. 1997, MNRAS, 289, 371
Vassiliadis, E., & Wood, P. R. 1993, ApJ, 413, 641